

PARAMETERIZATION OF HELICAL SUPERCONDUCTING UNDULATOR MAGNETIC FIELD*

S.H. Kim[†], Argonne National Laboratory, Argonne, IL 60439, USA

Abstract

Using a scaling law, the magnetic fields of helical superconducting undulators (HSCUs) for a period range of 10 – 50 mm are parameterized from the field calculations of one reference HSCU with a period of 30 mm. The on-axis fields are calculated at the critical current densities of the *NbTi* and *Nb₃Sn* superconducting coils at 4.2 K. The parametrized on-axis fields for the period range are expressed in terms of the period and inner radius of the helical coils. The corresponding critical current densities and coil maximum fields are also included. The parameterization procedures are described in detail and some field deviations are discussed.

INTRODUCTION

During the early phase of insertion device development, Halbach has provided the analytically derived on-axis field as a function of the pole gap and magnetic period for the use of pure permanent magnet blocks [1]. He also derived another on-axis field relation for the use of optimized samarium-cobalt alloy poles and magnet dimensions [2].

Using a wire of an infinitesimal cross section, the transverse field of a single helix is given by Smythe [3]. Kincaid has extended the field on the axis due to a pair of current carrying wires wound on a bifilar helix [4]. Assuming that the field pattern has a sinusoidal variation along the axis and no higher harmonics are present, Blewett and Chasman have derived the spiraling transverse field. [5].

The first helical superconducting undulator (HSCU) with a period of 30 mm was constructed by Elias and Madey in 1979 for an early free-electron laser experiment [6]. In recent years, short period HSCUs are under development at the Advanced Photon Source, Argonne National Laboratory, and several other institutions.

The on-axis field B_0 for the helical undulator with specific coil dimensions is expressed as

$$B_0 = \frac{2\mu_0 j \lambda}{\pi} \sin\left(k \frac{a}{2}\right) \int_{r_0}^{r_0+b} \{krK_0(kr) + K_1(kr)\} \frac{dr}{\lambda}. \quad (1)$$

Here μ_0 is the permeability in free space, j is the current in the coil pack on radius r_0 , $k = 2\pi/\lambda$ with λ as the undulator period along the z -axis, and K_0 and K_1 are modified Bessel functions [7]. The coil dimensions a and b are specified in Fig. 1.

Equation (1) suggests that when the undulator dimensions are scaled according to a period ratio and the $j\lambda$ is kept as a constant, the on-axis field B_0 remains unchanged. The more important aspect is that the whole field distribution remains unchanged even with non-linear magnetic poles. The scaling law must hold also for other electromagnets [8]. The units used in this paper are: length (mm), current (kA), and magnetic field (T).

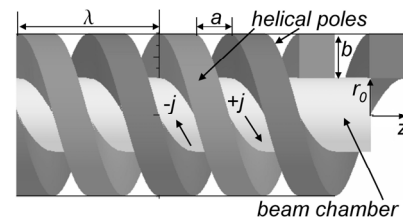


Figure 1: A model helical undulator: a double-helix steel coil is shown as magnetic poles on the outer surface of a beam chamber. In the empty space between the steel poles, helical coils of current densities, $+j$ and $-j$, are to be wound with r_0 as the inner radius of the coils, a and b as the coil dimensions.

THE SCALING LAW APPLICATION

As indicated in Eq. (1), when two undulator geometries are scaled, for example, 3:2, and the magnitude of the $j\lambda$ is kept as a constant, the undulators will have the same field distribution. For the reference undulator ($\lambda = 30$, $r_0 = 12$), the on-axis fields B_0 and the corresponding maximum field B_m in the superconducting (SC) coils in Fig. 2, along with the one that has been scaled down by a factor of 2/3 ($\lambda = 20$, $r_0 = 8$).

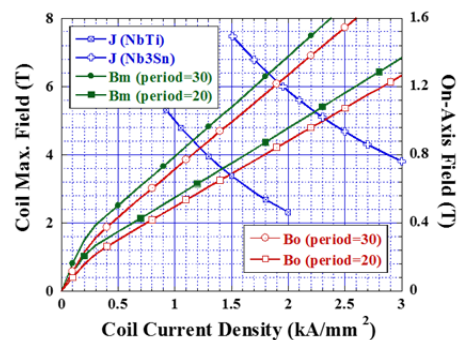


Figure 2: On-axis fields B_0 and maximum fields B_m in the coils are plotted as a function of coil (engineering) current density J for the two undulators with periods of 30.0 and 20.0.

*Work supported by the U.S. Department of Energy, Office of Science, under Contract No. DE-AC02-06CH11357

Associate of Seville, Advanced Photon Source

[†]shkim@aps.anl.gov, shkim242@gmail.com

Figure 2 shows that, within the calculation errors, the field values, B_m and B_0 , for $\lambda = 30$ at $J=1.0$ and 2.0 , for example, are the same as those for $\lambda = 20$ at $J=1.5$ and 3.0 , respectively. The fields with typical low-carbon steel poles were calculated using the Vector Fields Software [9].

As seen in Fig. 2, the steel poles are well saturated for $J > 0.5$ kA/mm², the fields for the two undulator are written in Eqs. (2a) and (2b). Equation (2c) is to calculate the on-axis field at about 80% of the critical current density. Equation (3) is a period ratio with $\lambda_{\text{ref}} = 30$. With $\lambda = 20$, Eqs. (2) represent for the 20 undulator. The period λ could be chosen any value within the specified range including the λ_{ref} .

$$B_m = (1.011 + 2.9442J)\lambda\text{ratio}, \quad (2a)$$

$$B_0 @ J_c = (0.16159 + 0.55342J)\lambda\text{ratio}, \quad (2b)$$

$$B_0 @ 0.8J_c = (0.16159 + 0.55342 * 0.8J)\lambda\text{ratio}. \quad (2c)$$

$$\lambda\text{ratio} = \frac{\lambda}{\lambda_{\text{ref}}}. \quad (3)$$

The current densities for the two SC coils at 4.2 K are based on the insulated wires at 5.0 T for the *NbTi* and at 12.0 T for the *Nb₃Sn* [10, 11]. The coil current densities J vs. B_m for the two SC coils are given by Eqs. (4a) and (4b) with the upper critical fields at 0 K: $B_{c1} = 10.6766$ T and $B_{c2} = 26.6547$ T.

$$J(\text{NbTi}) = (14.8249 / B_m)(1 - B_m / B_{c1})(B_m / B_{c1})^{0.6}, \quad (4a)$$

$$J(\text{Nb}_3\text{Sn}) = 1.54226(B_{c2} / B_m)^{0.5}(1 - B_m / B_{c2})^2. \quad (4b)$$

By using Eqs. (2a) and Eqs. (4), the J_c and B_m are calculated, and the corresponding B_0 may be calculated from Eqs. (2b) and (2c). By changing the period in Eq. (3), all the fields within the specified range of 10 – 50 mm can be calculated. It should be noted that when the period is changed for the calculations, the λ/r_0 ratio remains unchanged.

DEPENDENCE ON THE COIL RADIUS

The coil inner radius r_0 (12 mm) for the reference undulator is varied from 5 mm to 20 mm, and the calculated fields B_0 as a function of r_0 are plotted in Fig. 3. The exponential factor of the fields did not depend on the coil current densities of 1.5 ~ 3.5. For $J = 1.0$ and 0.5 the factors were increased only about 0.01% and 0.08%, respectively. The exponential variation was generalized into Eq. (5) to apply for the selected period range. It should be noted that when r_0 is less than 0.4λ , $f(r_0, \lambda)$ increases exponentially.

$$f(r_0, \lambda) = \exp[-0.9326(\frac{\lambda}{2\pi})(r_0 - \lambda / 2.5)]. \quad (5)$$

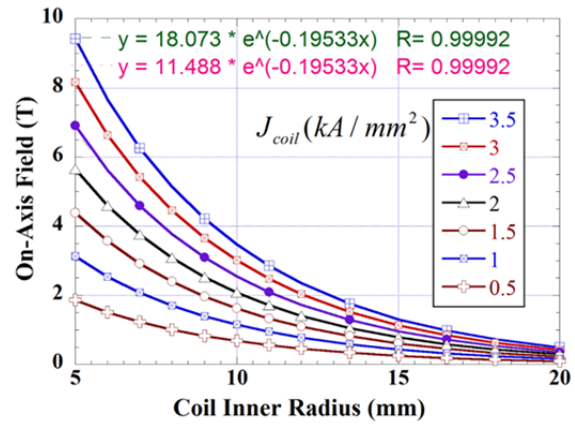


Figure 3: On-axis field dependence on the coil inner radius r_0 at seven coil current densities. As shown for the current densities at 2.5 and 1.5, the exponential factors of the field variations at different current densities are identical.

PARAMETERIZATION RESULTS

The calculated data from Eqs. (2) – (4) are plotted in Figs. (4) and (5). The results of the least square fits are listed in Eqs. (6) and (7) for the two *NbTi* and *Nb₃Sn* SC coils and Eq. (5), respectively. Without $f(r_0, \lambda)$ the two equations and figures imply that the undulator geometries within the period range are proportional to the reference undulator, $\lambda = 30$ mm and $r_0 = 12$ mm.

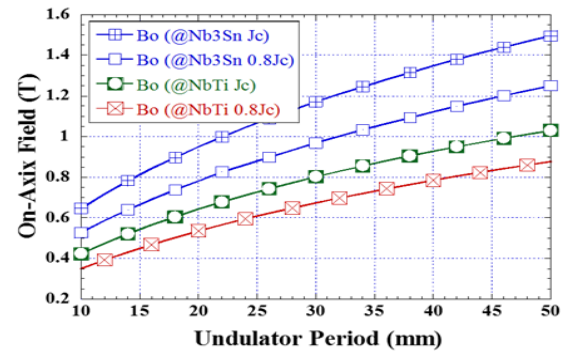


Figure 4: Plots of the on-axis fields from Eqs. (6) and (7) as a function of period, but not including Eq. (5).

$$B_0 @ J_c = (0.13652 + 0.033264\lambda - 4.586\lambda^2 10^{-4} + 3.0256\lambda^3 10^{-6})f(r_0, \lambda),$$

$$B_0 @ 0.8J_c = (0.10922 + 0.027689\lambda - 3.6689\lambda^2 10^{-4} + 2.4205\lambda^3 10^{-6})f(r_0, \lambda),$$

$$J_c = 2.8587 - 0.10727\lambda + 2.202\lambda^2 10^{-3} - 1.7491\lambda^3 10^{-5},$$

$$B_m @ J_c = 1.0336 + 0.14274\lambda - 9.8992\lambda^2 10^{-4}. \quad (6)$$

$$B_0 @ J_c = (0.25064 + 0.04592\lambda$$

$$-6.3725\lambda^2 10^{-4} + 4.3582\lambda^3 10^{-6})f(r_0, \lambda),$$

$$B_0 @ 0.8J_c = (0.19701 + 0.038284\lambda$$

$$-5.2652\lambda^2 10^{-4} + 3.6624\lambda^3 10^{-6})f(r_0, \lambda),$$

$$J_c = 4.6706 - 0.18567\lambda + 0.0039701\lambda^2 - 3.2024\lambda^3 10^{-5},$$

$$B_m @ J_c = 1.7768 + 0.19279\lambda - 1.3027\lambda^2 10^{-3}. \quad (7)$$

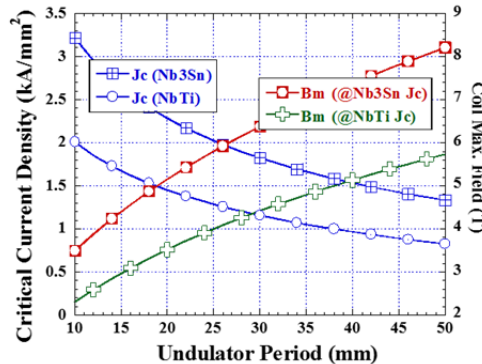


Figure 5: Plots of the critical currents and the corresponding maximum fields from Eqs. (6) and (7).

DEVIATION FROM THE RESULTS

Coil field for reduced $r_0=5$

For an extreme example, fields values at $r_0 = 5$ are compared with those of the reference $r_0 = 12$ in Fig.6. When r_0 is reduced from 12 to 5, B_0 increased by a factor of four times, but B_m increased less than 20%. Because of the increased B_m , when the B_0 values were calculated directly from the specific data, B_0 values were lower by about 7.7% for the *NbTi* and 8.15% for the *Nb₃Sn* compared to the parameterization results.

When the fields were calculated for $r_0 = 8$, corresponding to the above, differences were reduced to by about 4.9% and 4.7%, respectively.

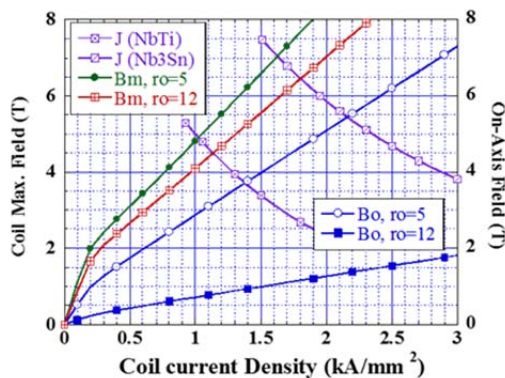


Figure 6: The on-axis field B_0 and coil maximum field B_m for the reference undulator and those for $r_0 = 5$ are plotted along with the current densities of the two SC coils.

Coil dimensions

The choice of the coil dimensions in Fig. 1, concerns the number turns and layers, as well as the conductor size, in order to optimize the coil packing factors, etc. A simple choice of the dimension may be about a quarter of the period length for the dimension parameters ($a \times b$). The coil dimensions (8×8) were used for the reference undulator.

An additional eight coil dimensions from (7×7) to (9×9) were selected, and calculated for the both kinds of the SC coils. When the calculated fields were compared with the (8×8) reference, the fields for the (7×7) coil were about 90.5% of the reference, and those for the (9×9) were about 105% of the reference.

CONCLUDING REMARKS

Though the field deviation shown in Fig. 6 is limited to extreme cases it may be worthwhile to develop the coil maximum field dependent on the coil radius, equivalent to Eq. (5).

REFERENCES

- [1] K. Halbach "Physical and optical properties of rare earth cobalt magnets," *Nucl. Instr. Meth.*, vol. 187, pp. 109-117, 1981.
- [2] K. Halbach "Permanent magnet undulators," *J. de Phys.*, vol. 44(C1), pp. 211-216, 1983.
- [3] W.R. Smythe, *Static and Dynamic Electricity* McGraw-Hill, New York, (1939) p. 272.
- [4] B.M. Kincaid, "A short-period helical wiggler as an improved source of synchrotron radiation," *J. Appl. Phys.*, Vol. 48, pp.2684-2691, 1977.
- [5] J.P. Blewett and R. Chasman "Orbits and fields in the helical wiggler," *J. Appl. Phys.*, vol. 48, pp2692-2698, 1977.
- [6] L.R. Elias and J.M. Madey, "Superconducting helically wound magnet for the free-electron laser," *Rev. Sci. Instr.*, vol. 50(11), pp. 1335-1340, 1979.
- [7] S.H. Kim, "Magnetic field analysis and achievable on-axis field for helical undulators," *Nucl. Instr. Meth.*, vol. A584, pp. 266-272, 2008.
- [8] S.H. Kim, "A scaling law for the magnetic fields of superconducting undulators," *Nucl. Instr. Meth.*, vol. A547, pp. 604-610, 2005.
- [9] Cobham Technical Services -Vector Fields Software, Oxford, UK. The author does not imply that a similar software by other vendors cannot perform the work.
- [10] M.S. Lubell, "Empirical scaling formulas for critical current and critical field for commercial NbTi," *IEEE Trans. Magn.*, vol. Mag -19, pp. 754-757, 1983.
- [11] L. T. Summers, M. W. Guinan, J. R. Miller, and P. A. Hahn, "A model for the prediction of Nb₃Sn critical current as a function of field, temperature, strain, and radiation damage," *IEEE Trans. Magn.*, vol. 27, pp. 2041-2044, 1991.